Chinese Chemical Letters 35 (2024) 108382

Contents lists available at ScienceDirect

Chinese Chemical Letters

journal homepage: www.elsevier.com/locate/cclet

Reshaping the imprinting strategy through the thermo-responsive moiety-derived "deep eutectic solvents" effect

Huihuang Xiong[a], Yiqun Wan[a,b,*], Yong Fan[b], Mengjia Xu[b], Aiping Yan[c], Yushan Zhang[d], Qifei Jiang[a], Hao Wan[a,*]

[a] State Key Laboratory of Food Science and Technology, Nanchang University, Nanchang 330047, China
[b] School of Chemistry and Chemical Engineering, Nanchang University, Nanchang 330031, China
[c] Jiangxi Province Key Laboratory of Modern Analytical Science, Nanchang University, Nanchang 330031, China
[d] Department of Computer Science, University of California Irvine, Irvine 92697, United States

ARTICLE INFO

Article history:
Received 14 December 2022
Revised 27 February 2023
Accepted 23 March 2023
Available online 26 March 2023

Keywords:
Deep eutectic solvents
Molecularly imprinted polymers
Magnetic
Thermo-responsive
Thermo-regulated elution

ABSTRACT

As a new concept having emerged in last few years, the "deep eutectic solvents" (DESs) effect integrated into the imprinting technology inevitably exposes design limitations of stimuli-responsive molecularly imprinted polymers (MIPs), as well as inadequate analysis of the adsorption performance of MIPs. Herein, a simple yet defined *N*-isopropylacrylamide/(3-acrylamidopropyl) trimethylammonium chloride (NIPAM/APTMAC) binary DESs system was proposed to prepare intelligent MIPs with thermo-sensitivity. Accordingly, magnetic and thermo-responsive MIPs based on functional monomers-derived DESs (TM-DESs-MIPs1) were synthesized, revealing DESs effect-regulated affinity/kinetics for the enhanced adsorption capability, eco-friendly thermo-regulated elution for high release efficiency, and simple magnetic separation, along with superior selectivity to rhein (RH) and good regeneration ability. TM-DESs-MIPs1 were utilized to extract RH from *Cassiae semen* samples coupled with high performance liquid chromatography (HPLC), yielding satisfactory recoveries (79.47%–110.82%) and low limits of detection (LOD) (16.67 μg/L). Another two kinds of MIPs adopting the thermo-responsive moiety-derived DESs effect strategy further demonstrated great applicability of such intelligent MIPs for analyses of complicated samples.

Sample pretreatment is always considered to be an essential part of the entire analytical procedure [1–3]. Specially, to combat the coronavirus disease 2019 (COVID-19) pandemic, Chinese medicine (CM) has appeared to be a promising alternative for patients [4,5], thus the extraction of components with bioactivity from CM has attracted increasing attentions. Commonly, adsorbents applied in sample pretreatment can be integrated with magnetic components, achieving rapid separation from samples by an external magnet [6–10]. Even so, some key challenges, such as poor selectivity and reusability of most adsorbents, time-consuming treatment processes, as well as the extensive consumption of toxic organic solvents cannot be ignored [11–13]. Therefore, there is a consistent need for developing an efficient and reliable extraction strategy.

Molecular imprinting technique (MIT) has been developed on the basis of simulating specific binding principles of enzymes-substrates or antibodies-antigens, involving the formation of tailor-made recognition sites within molecularly imprinted polymers (MIPs) [14–16]. The traditional MIPs with irregular shapes and deeply embedded recognition sites exhibit several inevitable shortcomings, such as imperfect removal of target molecules, destruction of recognition sites and large consumption of organic eluent [17,18]. Consequently, there is a great urgency to fabricate MIPs that facilitate the removal of template molecules, which were commonly found in combination with surface molecular imprinting technique or/and stimuli-responsive polymers [19]. Surface molecular imprinting anchors an imprinted layer on the matrix surface, ensuring easy accessibility to binding sites and fast mass transfer rate [20–22]. Meanwhile, stimuli-responsive MIPs (SR-MIPs) have demonstrated switchable features of binding/removal of target molecules upon external stimuli, providing convenient and eco-friendly protocols for separation/enrichment [23]. Stimuli-responsive components are usually adopted as functional monomers to synthesize SR-MIPs [24]. However, the limited kinds and number of functional monomers restrict further applications of SR-MIPs [25]. To date, exploring new functional monomers

* Corresponding authors.
E-mail addresses: wanyiqun@ncu.edu.cn (Y. Wan), wanhao424@ncu.edu.cn (H. Wan).

https://doi.org/10.1016/j.cclet.2023.108382
1001-8417/

to align with surface molecular imprinting and green stimuli responses is imperative for the cutting-edge imprinting strategy.

Deep eutectic solvents (DESs), a kind of green designer solvents [26], are formed from one or more hydrogen bond acceptors (HBAs) with one or more hydrogen bond donors (HBDs) at the proper ratio [27–30]. Although many DESs have been put forward as the functional monomers in the preparation of MIPs since 2016 due to the good extraction ability [31,32], such MIPs are still in infancy with few details on recognition properties associated with the DESs effect. In particular, the DESs-equipped functional monomers derived from a routine HBD or HBA are difficult to endow the MIPs with stimuli-sensitivity. Innovatively, we hypothesized that *N*-isopropylacrylamide (NIPAM), a representative monomer for the synthesis of thermo-responsive polymers, could serve as a HBD to team with a HBA to produce thermo-responsive moiety-derived DESs-equipped functional monomers for the fabrication of versatile MIPs with both DESs effect and thermo-responsiveness. It has been credibly reported that DESs-equipped functional monomers could improve the affinity of MIPs to target molecules in comparison with traditional functional monomers, resulting from the formation of multiple hydrogen bonds [33]. Furthermore, such imprinting strategy utilizing NIPAM-derived DESs effect enabled the intelligent MIPs to capture/release target analytes *via* temperature regulation, which is conducive to the application of MIPs in sustainable separation science.

Herein, we constructed a simple yet defined NIPAM/(3-acrylamidopropyl) trimethylammonium chloride (NIPAM/APTMAC) binary DESs system as functional monomers for the preparation of SR-MIPs. Rhein (RH), which could generate hydrogen bonds with the NIPAM-derived DESs, was selected as the template molecule for preliminary research. The obtained magnetic and thermo-responsive MIPs based on such DESs system (denoted as TM-DESs-MIPs1) were synthesized by surface molecular imprinting and systematically characterized. The DESs effect-regulated adsorption capacity, thermo-regulated elution efficiency, and selectivity of TM-DESs-MIPs1 were also investigated. TM-DESs-MIPs1 succeeded in serving as adsorbents of dispersive solid-phase extraction (d-SPE) coupled with high performance liquid chromatography (HPLC) for the efficient extraction and determination of RH from *Cassiae semen* samples. To demonstrate the universality of our new proposed imprinting strategy, another two kinds of MIPs (denoted as TM-DESs-MIPs2 and TM-DESs-MIPs3) were prepared by adopting such DESs-equipped functional monomers for effective analyses of triterpenoid saponins (*i.e.*, glycyrrhizic acid (GA)) and aristolochic acids (*i.e.*, aristolochic acid I (AAI)) from real samples. Consequently, such intelligent MIPs involving the thermo-responsive moiety-derived DESs effect feature rapid magnetic separation, high-affinity binding, eco-friendly thermo-regulated elution and favorable regeneration, indicating the potential applicability for selective extraction of analytes from complex samples and reshaping the MIT strategy for sample preparation.

The fabrication processes and the possible recognition mechanism of TM-DESs-MIPs1 were schematically illustrated in Fig. 1. The binary DESs system was a binary mixture formed by mixing NIPAM as a HBD and APTMAC as a HBA (molar ratio of 1:1) at 80 °C for 1 h [34]. The magnetic graphene (Mag@GO) coated with a silicon dioxide layer (denoted as Mag@GO@SiO_2) was obtained from the sequential solvothermal method and the sol-gel assembly [35]. Mag@GO@SiO_2 was modified with γ-methacryloxypropyltrimethoxysilane (MPS) (denoted as Mag@GO@SiO_2@MPS) to provide active sites for subsequent polymerization [36]. After using the binary DESs system as functional monomers and RH as the template molecule, the thermo-responsive imprinted layer was deposited onto the surface of Mag@GO@SiO_2. TM-DESs-MIPs1 were obtained with magnetic attraction after eluting the template molecules. The cavities imprinted by template molecules RH could provide a defined three-dimensional structure elusive to RH, achieving the selective recognition ability.

Transmission electron microscopy (TEM) and scanning electron microscope (SEM) images were shown in Fig. 2A and Fig. S1 (Supporting information). GO displayed a thin film with some wrinkles. Fe_3O_4 magnetic particles grown on GO sheets were spherical with the particle size of 323.1–393.8 nm. After the sol-gel assembly, a SiO_2 layer appeared around Mag@GO. The SEM images of TM-DESs-NIPs and TM-DESs-MIPs1 were similar, and the

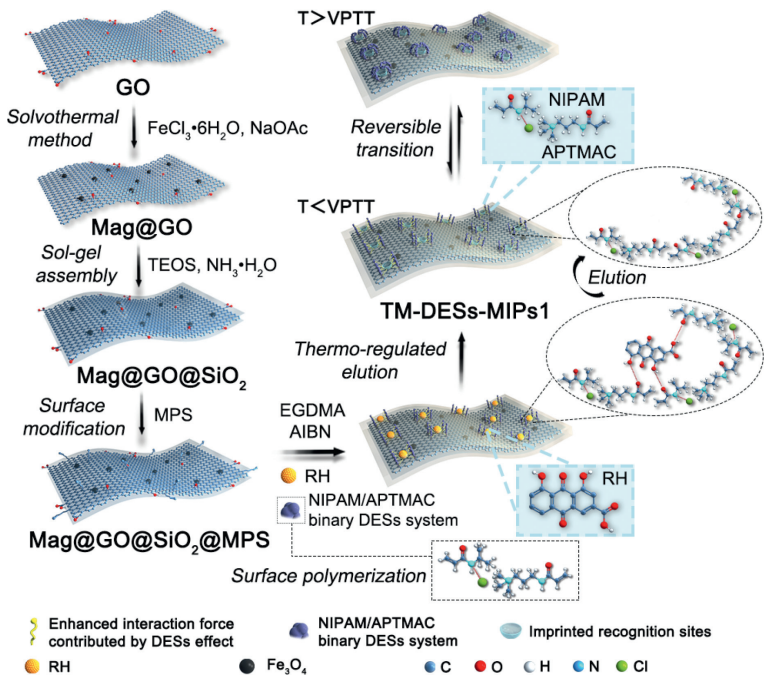

Fig. 1. Schematic illustration of the whole preparation and the possible recognition mechanism of TM-DESs-MIPs1.

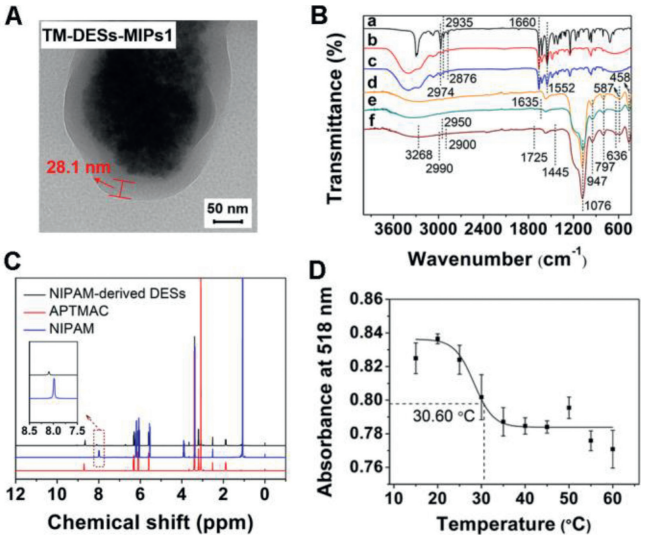

Fig. 2. (A) TEM image of TM-DESs-MIPs1. (B) FT-IR spectra of NIPAM (curve a), APTMAC (curve b), NIPAM-derived DESs (curve c), Mag@GO@SiO_2 (curve d), Mag@GO@SiO_2@MPS (curve e) and TM-DESs-MIPs1 (curve f). (C) ^{1}H NMR spectra of NIPAM, APTMAC and NIPAM-derived DESs. (D) The absorbance changes of TM-DESs-MIPs1 dispersed in MeOH at various temperatures.

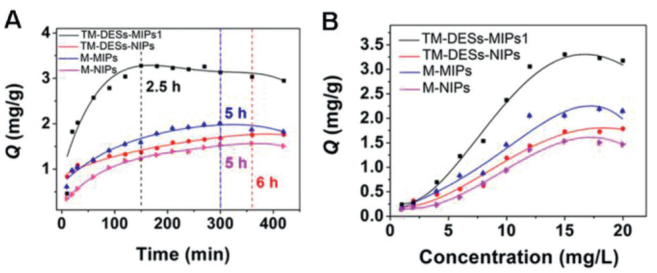

Fig. 3. (A) Dynamic adsorption and (B) static adsorption of TM-DESs-MIPs1, TM-DESs-NIPs, M-MIPs and M-NIPs.

wrinkled GO films existed on these materials. Finally, a thin imprinted layer with thickness of about 28.1 nm was formed near or on the surface of Mag@GO@SiO_2 after surface polymerization. Fig. 2B shows the results of Fourier transform infrared (FT-IR) spectra. Compared with NIPAM and APTMAC, the characteristic peaks of N–H (1552 cm^{-1}), C=C (1660 cm^{-1}), and C–H (2876–2974 cm^{-1}) were observed in NIPAM-derived DESs, verifying the successful design of the NIPAM/APTMAC binary DESs system. The broad peak (3300–3500 cm^{-1}) in both NIPAM-derived DESs and TM-DESs-MIPs1 was ascribed to the stretching vibration of O–H. In the spectrum of Mag@GO@SiO_2@MPS, in addition to stretching vibrations of Fe-O (587 cm^{-1}), Si-O-Si (1076 cm^{-1}), Si-O-H (947 cm^{-1}), Si-O (797 cm^{-1}) and Si-O-Fe (458 cm^{-1}) similar to those of Mag@GO@SiO_2, the stretching vibration of C=C and out of plane bending vibration of alkene C–H appeared at 1635 and 636 cm^{-1}, respectively, confirming the grafting of MPS. Collectively, stretching vibrations of C–H (2900–2990 cm^{-1}), C=O (1725 cm^{-1}) and N–H (3268 cm^{-1}), plus the bending vibration of C–H (1445 cm^{-1}) manifested that TM-DESs-MIPs1 were successfully synthesized. The binary DESs system was probed by ^{1}H NMR (Fig. 2C). The sharp and intensive H signal at 7.98 ppm shifted to 8.10 ppm of weak and broad band after the synthesis of NIPAM-derived DESs, which indicated that the micro-environment of hydrogen atoms in initial reactants had changed, probably resulting from the formation of hydrogen bonds within NIPAM-derived DESs [37]. From X-ray diffractometer (XRD) analysis (Fig. S2 in Supporting information), a sharp diffraction peak at 2θ=13° was indexed as (001) plane of GO [38], indicating that the graphite was stripped into a single layer of GO. The diffraction peaks of Fe_3O_4 at (311), (400), (422), (511) and (440) (JCPDS card No. 19–0629) confirmed that the anti-spinel structure of Fe_3O_4 was intact during the synthesis process [39]. As observed from Fig. S3 (Supporting information), the saturation magnetization values were 25.52 and 22.81 emu/g for TM-DESs-MIPs1 and TM-DESs-NIPs, respectively, which would facilitate magnetic separation and reusability. The thermal stability of relative materials was tested by thermogravimetric analyses (TGA) (Fig. S4 in Supporting information), and TM-DESs-MIPs1 demonstrated good thermo-stability in practical applications. The volume phase transition temperature (VPTT) of the TM-DESs-MIPs1 was defined as the temperature at which a half decrease of maximum value of optical absorption variation as a function of temperature occurred, corresponding to the phase transition of thermosensitive polymers [40]. From the results of UV–vis (Fig. 2D), the absorbance of TM-DESs-MIPs1 in methanol (MeOH) decreased with the increment of temperature, and when the value was exactly half of the total absorbance change, the VPTT of TM-DESs-MIPs1 was 30.60 °C in MeOH, suggesting that TM-DESs-MIPs1 would undergo a reversible swollen/shrunk state as a result of temperature responsiveness [35].

Since there are few reports on the impact of DESs-equipped functional monomers on the adsorption performance of MIPs, comparative materials TM-DESs-NIPs (with DESs effect, but without imprinted recognition sites), M-MIPs (without DESs effect, but with imprinted recognition sites), and M-NIPs (without DESs effect and imprinted recognition sites) were specially prepared to assess the DESs effect-regulated adsorption properties of TM-DESs-MIPs1 (see Fig. S5 for a brief description and the Experimental Methods in Supporting information for the details). In terms of the adsorption kinetics (Fig. 3A), it took only 2.5 h for TM-DESs-MIPs1 to reach the maximum adsorption capacity, in a strike contrast to 6 h for the case of TM-DESs-NIPs, which was attributed to the deficiency of specific binding cavities. Comparatively, it took twice the time (5 h) of the case of TM-DESs-MIPs1 for both M-MIPs and M-NIPs to reach the adsorption saturation, possibly due to the absence of the NIPAM-derived DESs effect. Compared with M-NIPs, TM-DESs-NIPs and M-MIPs, the adsorption efficiency of TM-DESs-MIPs1 increased by 94.78%–261.04%, 67.29%–138.84% and 56.14%–114.61% within the evaluation timeframe, respectively (Fig. S6A in Supporting information). Apparently, DESs effect within TM-DESs-MIPs1 could cooperate with the molecular recognition of imprinted sites to facilitate the adsorption process.

The static adsorption experiments were further conducted to evaluate the DESs effect-regulated adsorption capacity of TM-DESs-MIPs1 at various concentrations of RH (Fig. 3B). The equilibrium adsorption capacity of TM-DESs-MIPs1 was about 3.30 mg/g. Since there were no vacant binding sites in TM-DESs-NIPs and M-NIPs, their adsorption capacities were unsatisfactory. In addition, M-MIPs showed similar adsorption trends as TM-DESs-MIPs1, but the adsorption capacity was lower, which may be due to the lack of the DESs effect. When the concentration ranged from 4 mg/L to 20 mg/L, the adsorption efficiency of TM-DESs-MIPs1 increased by 114.49%–213.32%, 57.90%–147.39%, and 36.78%–75.61% in comparison with M-NIPs, TM-DESs-NIPs and M-MIPs, respectively (Fig. S6B in Supporting information), which was consistent with the results of the dynamic adsorption. To sum up, such thermo-responsive moiety-derived DESs system demonstrated to be an effective candidate of functional monomers for the preparation of intelligent MIPs to accelerate the adsorption process and enhance the adsorption capacity.

The selectivity of TM-DESs-MIPs1 was investigated by using aurantio-obtusin, obtusin, emodin, chrysophanol and physcion as competitors of RH (Figs. S7 and S8 and Table S1 in Supporting in-

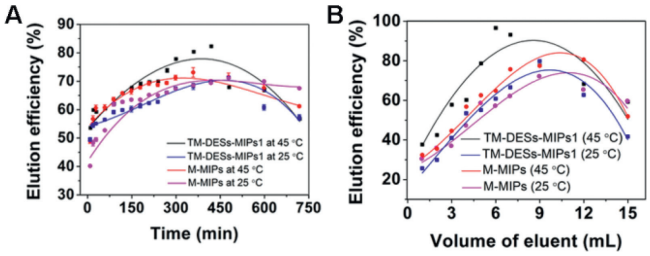

Fig. 4. The elution efficiency of TM-DESs-MIPs1 and M-MIPs under different elution time (A) and using different volume of eluent (B) at 45 °C or 25 °C.

formation). TM-DESs-MIPs1 exhibited the highest binding capacity for RH compared with other competitive substances. The values of selectivity factors (β) of TM-DESs-MIPs1 for RH against five analogues ranged from 2.38 to 5.22, which were higher than the β values ($\geq$1.37) of MIPs in previously reported studies [4]. According to the analysis of variance (ANOVA) post-hoc least significant difference (LSD) test [11], the adsorption capability of TM-DESs-MIPs1 for other competitive substances obviously decreased ($P < 0.001$) compared with RH. Besides, TM-DESs-MIPs1 performed the highest value of imprinting factors (α) for RH, accompanying with better extraction efficiency than TM-DESs-NIPs1. Therefore, TM-DESs-MIPs1 possessed high selectivity to RH.

Since the thermo-sensitive property of TM-DESs-MIPs1 was essentially derived from the temperature-dependent phase transition of poly (NIPAM) (PNIPAM) [40,41], the control imprinting material M-MIPs without PNIPAM were employed to assess the superiorities of thermo-regulated elution (see the Experimental Methods in Supporting information). As depicted in Fig. 4A, when the ambient temperature was 45 °C (beyond VPTT), most RH (82.28%) was desorbed from TM-DESs-MIPs1 within 7 h, while the elution efficiency of M-MIPs was less than 70.00% at the same time. It took 6 h for M-MIPs to attain the elution efficiency of 73.11% (the maximum efficiency), about 2 h longer than TM-DESs-MIPs1 to achieve the similar efficiency. The elution efficiency of TM-DESs-MIPs1 at 45 °C was apparently better than that of TM-DESs-MIPs1 at 25 °C (below VPTT) at various time points. However, for M-MIPs, the elution efficiency at 45 °C was only slightly better than that at 25 °C, which may be driven by the molecular thermal motion that was conducive to the desorption of RH.

As for eluent volume (Fig. 4B), M-MIPs demanded about 12 mL of eluent to attain its maximum elution efficiency (80.41%) at 45 °C, whereas TM-DESs-MIPs1 only consumed half amount (6 mL) of eluent to obtain the maximum efficiency of 96.56%, demonstrating to be eco-friendlier and more efficient. Compared with M-MIPs, the discrepancy of elution efficiency of TM-DESs-MIPs1 at 45 °C and 25 °C was more obvious. Owing to the lack of temperature-dependent volume phase transition property, the elution efficiency of M-MIPs maintained at a moderate level even large eluent volume was applied [42]. Briefly, when the ambient temperature was 45 °C (beyond VPTT), the structures of thermo-sensitive polymers in TM-DESs-MIPs1 collapsed, realizing the high-efficiency release of target components. As depicted from Figs. 4A and B, there was a decline in elution efficiency if the elution time and eluent volume continued to increase to a certain extent, which may be attributed to over elution causing the target analytes to rebind to vacant imprinted sites to reach a dynamic equilibrium. Similar phenomena have also been observed in recent published research [43–45]. Moreover, the broad ranges of elution time and the volume of eluent intuitively reflected that the thermo-regulated elution of TM-DESs-MIPs1 demonstrated superiorities of short elution time and low organic-solvent consumption, surpassing the direct organic-solvent elution of the conventional MIPs to conform to the concept of "green chemistry". The aforementioned advantages of TM-DESs-MIPs1 were more obvious than those of our published conventional thermo-sensitive MIPs [35], which revealed the potential of intelligent elution of TM-DES-MIPs1 with the introduction of NIPAM-derived DESs system.

Under the optimized conditions of d-SPE procedure (see the Experimental Methods and Fig. S9 in Supporting information), the proposed TM-DESs-MIPs(1-3)-HPLC methods were valuated from the aspects of linearity, limits of detection (LOD), limits of quantification (LOQ), accuracy and precision (Table S2 in Supporting information). The calibration curves were attained within the ranges of 0.08–8 mg/L for RH, 1.5–60 mg/L for GA and 0.2–10 mg/L for AAI, with correlation coefficients (R) between 0.9936 and 0.9986. The LODs of these methods for RH, GA and AAI were 16.67, 363.64 and 37.52 μg/L, respectively, which were lower than those of the reported literatures [46–48]. The recoveries of TM-DESs-MIPs(1-3) for the above analytes in CM samples at three spiked levels (*Cassiae semen* and *Aristolochia fangchi* spiked at 0.5, 2.0, and 5.0 mg/L, *Glycirrhiza glabra* spiked at 5.0, 10.0 and 20.0 mg/L) were 87.66%–106.41%. The relative standard deviations (RSDs) for the inter-day and intra-day precisions were less than 7.26% and 6.16%, respectively, indicating the steady extraction performance of the intelligent materials. In addition, TM-DESs-MIPs(1-3) showed favorable regeneration ability with a recovery rate around 88.41% even after seven adsorption-desorption cycles (Fig. S10 in Supporting information).

To validate the robustness of the thermo-responsive moiety-derived DESs imprinting strategy, the optimized methods were employed for the extraction of analytes in CM samples grew from different regions. The pristine samples were spiked with above analytes at three levels. The recoveries achieved by TM-DESs-MIPs1 ranged from 79.47% to 110.82% with RSDs of 2.34%–7.83% for *Cassiae semen*, surpassing over those of TM-DESs-NIPs (19.26%–45.05%) with RSDs of 1.62%–7.27% (Fig. 5A). As for TM-DESs-MIPs2 and TM-DESs-MIPs3, satisfactory recoveries were obtained in the ranges of 80.92%–105.08% for *Glycirrhiza glabra*, and 81.92%–102.80% for *Aristolochia fangchi*, respectively (Fig. S11 in Supporting information). However, TM-DESs-NIPs exhibited lower recovery rates. As seen in Fig. 5B and Fig. S12 (Supporting information), compared with the spiked samples, target analytes were remarkably concentrated after the extraction by TM-DESs-MIPs(1-3). In a strike contrast, TM-DESs-NIPs showed poor extraction behavior, reflecting the efficient imprinting ability of our strategy.

In summary, a simple yet defined NIPAM/APTMAC binary DESs system was used as functional monomers to prepare intelligent MIPs. TM-DESs-MIPs1 demonstrated superior adsorption capacity

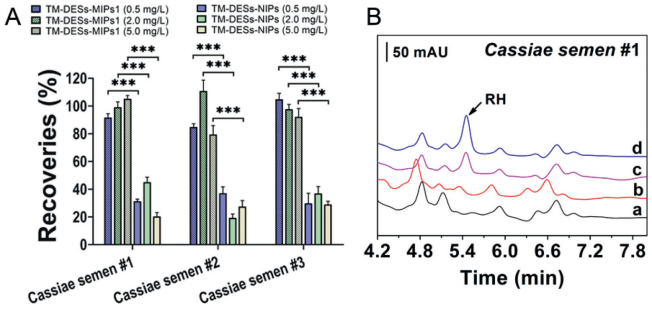

Fig. 5. (A) The recoveries of TM-DESs-MIPs1 and TM-DESs-NIPs for RH in the spiked *Cassiae semen* samples. *Cassiae semen* samples (#1 to #3 represented different habitats of Linyi city, Shandong province, Bozhou city, Anhui province, and Zhumadian city, Henan province, respectively). Data were expressed as the mean ± SD (n=3). ***$P < 0.001$ (recoveries of TM-DESs-MIPs1 for RH compared with that of TM-DESs-NIPs). (B) HPLC chromatograms of pristine *Cassiae semen* #1 (curve a), the samples spiked at 2.0 mg/L (curve b), and the spiked samples were extracted by TM-DESs-NIPs (curve c) and TM-DESs-MIPs1 (curve d).

and fast binding kinetics to RH attributed to the DESs effect and imprinted cavities, along with rapid magnetic separation, surpassing the comparative materials M-MIPs, TM-DES-NIPs and M-NIPs. Unlike the direct organic-solvent elution conventionally applied in M-MIPs, the thermo-regulated elution of TM-DESs-MIPs1 exhibited shorter elution time and lower organic-solvent consumption. Another two kinds of MIPs with such DESs effect further revealed the universality of our new proposed imprinting strategy. This study was an attempt to explore novel SR-MIPs with the thermo-responsive moiety-derived DESs effect, providing a convenient and eco-friendly application prospect for the extraction of trace analytes in complex samples.

Declaration of competing interest

The authors declare that they have no known competing financial interests or personal relationships that could have appeared to influence the work reported in this paper.

Acknowledgments

This work was supported by National Key Research and Development Project (No. 2019YFC1604904), National Natural Science Foundation of China (No. 32101212), Natural Science Foundation of Jiangxi (No. 20224ACB215009), and Research Program of State Key Laboratory of Food Science and Technology in Nanchang University (No. SKLF-ZZB-202127).

Supplementary materials

Supplementary material associated with this article can be found, in the online version, at doi:10.1016/j.cclet.2023.108382.

References

[1] Y. Li, S. Lan, T. Zhu, Trends Analyt. Chem. 142 (2021) 116319.
[2] J. Yang, Y. Chen, K. Shi, et al., Chin. Chem. Lett. 33 (2022) 3444–3450.
[3] X. Bao, J. Liu, Q. Zheng, et al., Chin. Chem. Lett. 30 (2019) 2266–2270.
[4] J. Li, R. Dong, X. Wang, et al., RSC Adv. 5 (2015) 10611–10618.
[5] S. Shi, F. Wang, J. Li, et al., IUBMB Life 73 (2021) 739–760.
[6] Z. Yu, L. Huang, Z. Zhang, et al., Chin. Chem. Lett. 33 (2022) 3853–3858.
[7] W. Jing, J. Wang, B. Kuipers, et al., Trends Analyt. Chem. 137 (2021) 116212.
[8] M. Zark, U. Riebesell, T. Dittmar, Sci. Adv. 1 (2015) e1500531.
[9] Z. Liu, Y. Zhou, M. Guo, et al., J. Hazard. Mater. 371 (2019) 712–720.
[10] H. Qi, L. Jiang, Q. Jia, Chin. Chem. Lett. 32 (2021) 2629–2636.
[11] X. Mao, W. Xiao, Y. Wan, et al., Food Chem. 345 (2021) 128807.
[12] Y. Wang, Q. Ye, M. Yu, et al., Chin. Chem. Lett. 31 (2020) 1843–1846.
[13] C. Wu, T. Li, D. Li, et al., Chin. Chem. Lett. 32 (2021) 2174–2178.
[14] O.I. Parisi, M. Dattilo, F. Patitucci, et al., Nanoscale 13 (2021) 16885–16899.
[15] S.P.B. Teixeira, R.L. Reis, N.A. Peppas, et al., Sci. Adv. 7 (2021) eabi9884.
[16] Z. Xu, X. Jiang, S. Liu, et al., Chin. Chem. Lett. 31 (2019) 185–188.
[17] J. Ma, L. Jiang, G. Wu, et al., J. Chromatogr. A 1466 (2016) 12–20.
[18] Y. Ma, Y. Zhang, M. Zhao, et al., Chem. Commun. 48 (2012) 6217–6219.
[19] Q. Zhao, H. Zhao, W. Huang, et al., Anal. Methods 11 (2019) 2800–2808.
[20] D. Wu, W. Baaziz, B. Gu, et al., Nat. Catal. 4 (2021) 595–606.
[21] N. Zhao, Z. Liu, J. Xing, et al., Chin. Chem. Lett. 33 (2022) 3031–3034.
[22] M. Chen, H. Yang, Y. Si, et al., Food Chem. 355 (2021) 129656.
[23] H. Xiong, L. Guo, X. Mao, et al., Food Chem. 331 (2020) 127311.
[24] M. Arabi, A. Ostovan, J. Li, et al., Adv. Mater. 33 (2021) 2100543.
[25] L. Chen, X. Wang, W. Lu, et al., Chem. Soc. Rev. 45 (2016) 2137–2211.
[26] L. Peng, Z. Hu, Q. Lu, et al., Chin. Chem. Lett. 30 (2019) 2151–2156.
[27] T. Gu, M. Zhang, J. Chen, et al., Chem. Commun. 51 (2015) 9825–9828.
[28] L. Li, K. Liu, H. Xing, et al., J. Catal. 374 (2019) 306–319.
[29] J. Chen, M.C. Ali, R. Liu, et al., Chin. Chem. Lett. 31 (2020) 1584–1587.
[30] H. Zhang, Y. Wang, K. Xu, et al., Anal. Methods 8 (2016) 8196–8207.
[31] Y. Liu, Y. Wang, Q. Dai, et al., Anal. Chim. Acta 936 (2016) 168–178.
[32] L. Tan, L.D. Zhou, Z.F. Jiang, et al., J. Pharm. Biomed. Anal. 192 (2021) 113661.
[33] G. Li, W. Wang, Q. Wang, et al., J. Chromatogr. Sci. 54 (2016) 271–279.
[34] Z. Liu, Y. Wang, F. Xu, et al., Anal. Chim. Acta 1129 (2020) 49–59.
[35] H. Xiong, Y. Fan, X. Mao, et al., Food Chem. 372 (2022) 131250.
[36] X. Kan, Y. Zhao, Z. Geng, et al., J. Phys. Chem. C 112 (2008) 4849–4854.
[37] H. Lü, S. Wang, C. Deng, et al., J. Hazard. Mater. 279 (2014) 220–225.
[38] L. Yan, Y. Yin, P. Lv, et al., J. Agric. Food Chem. 64 (2016) 3091–3100.
[39] X. Ding, Y. Wang, Y. Wang, et al., Anal. Chim. Acta 861 (2015) 36–46.
[40] L. Xu, J. Pan, J. Dai, et al., J. Hazard. Mater. 233-234 (2012) 48–56.
[41] W. Huang, P. Xu, W. Yang, et al., RSC Adv. 6 (2016) 74734–74741.
[42] E.A. Dil, A. Asfaram, H. Javadian, J. Chromatogr. B: Anal. Technol. Biomed. Life Sci. 1158 (2020) 122249.
[43] Y. Yang, Y. Sun, H. Chen, et al., Anal. Methods 12 (2020) 507–513.
[44] W. Lu, W. Ming, X. Zhang, et al., Electrophoresis 37 (2016) 2487–2495.
[45] H.I. Ulusoy, E. Yılmaz, M. Soylak, Microchem. J. 145 (2019) 843–851.
[46] D. Li, S. Liu, Y. Shen, et al., Luminescence 30 (2015) 60–66.
[47] A.K. De, S. Datta, A. Mukherjee, J. Adv. Pharm. Technol. Res. 3 (2012) 210–215.
[48] J. Ye, X. Cai, Q. Zhou, et al., Microchim. Acta 187 (2020) 623.